


Article

Absolute Distance Measurement Based on Self-Mixing Interferometry Using Compressed Sensing

Li Li ^{1,2,3} , Yue Zhang ⁴, Ye Zhu ^{1,2}, Ya Dai ^{1,2}, Xuan Zhang ^{1,2,5} and Xuwen Liang ^{1,2,3,*}

¹ Innovation Academy for Microsatellites of CAS, Shanghai 201204, China

² Shanghai Engineering Center for Microsatellites, Shanghai 201204, China

³ University of Chinese Academy of Sciences, Beijing 100049, China

⁴ China Telecom Research Institute, Shanghai 200122, China

⁵ Hefei National Laboratory, Hefei 230088, China

* Correspondence: 18217631362@163.com

Abstract: An absolute distance measurement sensor based on self-mixing interferometry (SMI) is suitable for application in aerospace due to its small size and light weight. However, an SMI signal with a high sampling rate places a burden on sampling devices and other onboard sources. SMI distance measurement using compressed sensing (CS) is proposed in this work to relieve this burden. The SMI signal was sampled via a measurement matrix at a sampling rate lower than Nyquist's law and then recovered by the greedy pursuit algorithm. The recovery algorithm was improved to increase its robustness and iteration speed. On a distance measuring system with a measurement error of 60 μm , the difference between raw data with 1800 points and CS recovered data with 300 points was within 0.15 μm , demonstrating the feasibility of SMI distance measurement using CS.

Keywords: self-mixing interferometry; distance measurement; compressed sensing; recovery algorithm



Citation: Li, L.; Zhang, Y.; Zhu, Y.; Dai, Y.; Zhang, X.; Liang, X. Absolute Distance Measurement Based on Self-Mixing Interferometry Using Compressed Sensing. *Appl. Sci.* **2022**, *12*, 8635. <https://doi.org/10.3390/app12178635>

Academic Editor: Alberto Gatto

Received: 24 July 2022

Accepted: 26 August 2022

Published: 29 August 2022

Publisher's Note: MDPI stays neutral with regard to jurisdictional claims in published maps and institutional affiliations.



Copyright: © 2022 by the authors. Licensee MDPI, Basel, Switzerland. This article is an open access article distributed under the terms and conditions of the Creative Commons Attribution (CC BY) license (<https://creativecommons.org/licenses/by/4.0/>).

1. Introduction

The self-mixing phenomenon refers to the effect in which an emitted laser beam is partially reflected by a target and mixed with the light inside the laser cavity, resulting in modulation of both the output laser power and the optical frequency [1]. The modulated power or modulated frequency can be used to estimate the target's properties. A measurement sensor with SMI does not require a beam splitter, reference mirror, and external photodetector, so it has the characteristics of low cost, simplicity and compact structure. SMI sensors are widely used in the field of distance [2,3], displacement [4,5], vibration [6,7], and velocity [8,9] measurements. Moreover, the use of laser diodes as a light source can further reduce size and weight [2,10]. These benefits make SMI-based sensors suitable for deployment as nodes in a measurement network. For example, distance measurement sensors based on SMI can be used to monitor the structural deformation of space optical communication satellites or quantum satellites, which have strict requirements for precise structures.

Most already reported methods for SMI distance sensing depend on the beat frequency of fringes induced by linear current modulation, due to the approximate linear relation between beat frequency and distance [2]. The fringe-counting method [11] in the time domain and the spectrum analysis method [12] in the frequency domain are commonly used to obtain the beat frequency. When compared, the spectrum analysis method achieves higher measurement accuracy and can adapt to measurements with a lower signal-to-noise ratio [13,14]; therefore, most signal-processing work for SMI distance measurement focused on spectrum estimation algorithms to obtain the modulated frequency.

A high sampling rate for distance measurement is set to ensure accuracy and a wide range of measurements. The high sampling rate places a burden on sampling device capability, energy consumption, data transmission capability, and data storage capacity,

which are sensitive to sensor nodes or satellites with limited resources [15]. To address this issue, compression algorithms are typically applied to satellites to reduce data size [16,17]. However, they do not fundamentally solve the problem. Compression algorithms place an additional computational burden on satellites, and the demand for sampling devices with a high sampling rate is not alleviated.

In the traditional sampling approach based on the Nyquist sampling theorem, a large effort is made to obtain complete information at the sampling stage, and useless information is discarded at the compression stage. Unlike the traditional approach, the novel theory of compressed sensing (CS) provides a new approach for data acquisition and data compression at the same time [18]. In the CS method, fewer data are sampled at the satellite, reducing the burden on sampling devices and subsequent transmission. No other complex computations are required at the satellite, and the recovery algorithm for sampled data is implemented on the ground with ample computing resources. The CS theory works on the premise that if a signal is sparse in some transform domain, far fewer measurements are needed to reconstruct the signal compared to the Nyquist sampling theorem [19]. The SMI signal is cosine-like, with only a few indexes of the spectrum having non-zero values. When spectrum estimation algorithms are utilized for SMI distance measurement, only the index corresponding to the maximum amplitude and a few other indexes are concerned [20]. Therefore, the SMI signal can be regarded as a sparse signal in the Fourier domain. In light of this, we used CS for SMI distance measurement in our work.

2. Theoretical Analysis

2.1. Self-Mixing Interferometry

SMI can be interpreted using a three-facet Fabry–Perot cavity and simplified using a two-facet Fabry–Perot cavity [10]. Neglecting multiple reflections and under a weak feedback level, the modulated power P and the modulated frequency ν_F can be expressed as

$$\frac{4\pi L}{c}(\nu_0 - \nu_F) = C \sin\left(\frac{4\pi L}{c}\nu_F + \arctan\alpha\right), \quad (1)$$

$$P = P_0[1 + m \cos\left(\frac{4\pi L}{c}\nu_F\right)], \quad (2)$$

where L is the distance between the external target and the laser's front mirror, ν_0 is the optical frequency without feedback, m is the modulation coefficient, and c is the speed of light. C is the external feedback strength parameter related to external distance, length of the laser internal cavity, and reflectivity of the laser front mirror and the external target. C is an important parameter that affects the dynamics of the laser as well as its output power P . A weak feedback level ($C < 1$) gives a single solution in Equation (1) and causes ν_F to approximate ν_0 [21]. When the laser is linearly modulated above its threshold by a direct current with a sawtooth wave current, the modulated power P in Equation (2) can be expressed as

$$\begin{aligned} P(t) &\approx P_0 + P_0 m \cos\left\{\frac{4\pi L}{c}[\nu_0 + \gamma tr(t)]\right\} \\ &= P_0 + P_0 m \cos\left\{\frac{4\pi L \gamma r(t)}{c}t + \frac{4\pi L}{c}\nu_0\right\} \\ &= P_0 + P_0 m \cos(2\pi ft + \varphi) \end{aligned} \quad (3)$$

where γ means the modulation relationship between lasing frequency and modulation current with a unit Hz/mA, which is always considered constant in distance measurement. The parameter $r(t)$ represents the slope of the sawtooth wave current.

Both the frequency and the phase of the SMI power signal contain external distance L . However, the problem of phase ambiguity occurs when the phase is used to obtain the distance, so that the accurate distance cannot be distinguished. Therefore, the frequency of the SMI signal is usually extracted to obtain external distance via

$$L = \frac{fc}{2\gamma r(t)}. \quad (4)$$

Because of the excellent properties of the fast Fourier transform (FFT), it is commonly used to calculate frequency. Given that the accuracy of frequency measurement directly impacts the accuracy of distance measurement, some spectrum correction methods are used to overcome the picket fence effect. Interpolated FFT [20] is one of these methods, and is widely used due to its ease of implementation and high correction accuracy. The correction method for interpolated FFT using the Hanning window is defined as

$$\hat{f} = \frac{f_s}{N} \left(k^* \pm \frac{2A_{k^* \pm 1} - A_{k^*}}{A_{k^* \pm 1} + A_{k^*}} \right), \quad (5)$$

where f_s is the sampling rate, N is the number of sampling points, k^* is the index of the maximum peak, and A_{k^*} and $A_{k^* \pm 1}$ are the amplitudes of the maximum peak and lateral peaks respectively. The sign of the inner sum in Equation (5) depends on the amplitude of the lateral peaks. The sign “+” is used when A_{k^*+1} is greater than A_{k^*-1} , and when vice versa, “−” is used.

2.2. Compressed Sensing

A signal $\mathbf{x} \in \mathbb{R}^N$ can be expressed as a weighted sum of the columns of an orthonormal basis matrix $\Psi \in \mathbb{R}^{N \times N}$, via

$$\mathbf{x} = \Psi \mathbf{s}, \quad (6)$$

where $\mathbf{s} \in \mathbb{R}^N$ is the weight coefficient. This signal can be called K -sparse on a sparse basis Ψ if there are no more than K ($K < N$) nonzero elements in \mathbf{s} . The sparse basis can be Fourier basis, wavelet basis, cosine basis, etc. A suitable sparse basis should be selected to minimize the number of nonzero elements to obtain the best sparse representation. In CS theory, a sparse signal can be sampled by a measurement matrix $\Phi \in \mathbb{R}^{M \times N}$ where $M < N$ to obtain the signal $\mathbf{y} \in \mathbb{R}^M$. The sampling process can be denoted with

$$\mathbf{y} = \Phi \mathbf{x} = \Phi \Psi \mathbf{s} = \Theta \mathbf{s}, \quad (7)$$

where matrix $\Theta \in \mathbb{R}^{M \times N}$ denotes the sensing matrix. The matrix Θ needs to satisfy the Restricted Isometry Property (RIP) [22] so that the sampled vector \mathbf{y} can preserve sufficient information to fully recover the original signal \mathbf{x} . It has been proven that the sensing matrix Θ can satisfy the RIP when the measurement matrix Φ is a Gaussian matrix, Bernoulli matrix, Fourier random matrix, or Hadamard matrix [23].

Signal reconstruction will be conducted after measurement and is formulated as an ℓ_0 norm minimization problem. The unknown K -sparse vector can be reconstructed via

$$\min_{\mathbf{s}} \|\mathbf{s}\|_0 \text{ s.t. } \mathbf{y} = \Phi \Psi \mathbf{s}, \quad (8)$$

where $\|\bullet\|_p = (\sum_1^n |\bullet|)^{1/p}$ denotes the ℓ_p -norm. The ℓ_0 -minimization is NP-hard, in general. There are usually two methods for resolving this issue. The first is ℓ_1 -minimization and the second is greedy pursuit algorithms. It has been demonstrated that ℓ_1 -minimization can replace ℓ_0 -minimization when the sensing matrix Θ satisfies the RIP [24]. The main advantage of ℓ_1 -minimization is that it is a convex optimization problem, and therefore, linear programming technologies can be used to solve the function. However, ℓ_1 -minimization has high computational complexity. In comparison, greedy pursuit algorithms have a favorable computational profile. The main idea of greedy pursuit is to select the most valuable columns, called atoms, from the sensing matrix and then gradually reconstruct the signal. Orthogonal matching pursuit (OMP) [25] is a widely used greedy pursuit algorithm.

2.3. SMI Distance Measurement Using CS

In comparison to the traditional sampling method, the CS method employs non-uniform sampling based on the measurement matrix and incorporates a signal recovery

process. Figure 1 depicts block diagrams of the traditional sampling method and the CS method for SMI distance measurement.

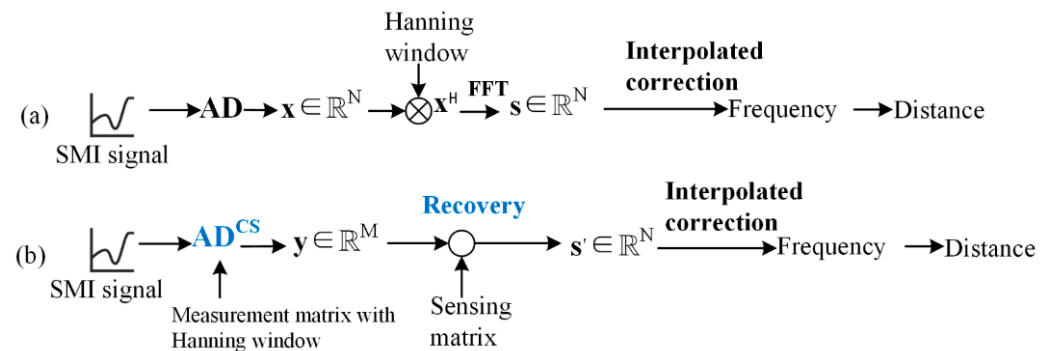


Figure 1. Block diagrams for SMI distance measurement: (a) Traditional method; (b) CS method.

In the traditional spectrum estimation method, the SMI signal is acquired by analog-to-digital (AD) conversion. Following that, FFT and interpolated correction are applied to the sampled signal with the Hanning window added. The modulated frequency in Equation (3) can be obtained, and the external distance calculated, according to Equation (4). In the CS method, signal y with fewer points than in the traditional method is sampled through control of the measurement matrix, which can be implemented by a demodulator [26]. To reduce spectral leakage as in traditional methods, a Hanning window is multiplied on each row of the measurement matrix. After that, the recovery coefficient vector s' can be solved using the recovery algorithm. The following steps in the CS method are consistent with the traditional method. In our work, the widely used Gaussian matrix was selected as measurement matrix to facilitate analysis, and the CS sampling process was simplified into the multiplication of the original signal and the measurement matrix. The OMP algorithm was used as the signal recovery algorithm for SMI distance measurement.

When the Fourier basis is used as a sparse matrix and OMP is selected as the recovery algorithm, two improvements were made in our work regarding acceleration and robustness.

- Acceleration

Conjugate symmetry is present in the Fourier transform of real numbers. This feature can be used to accelerate the OMP recovery algorithm. When a column in the sensing matrix achieves its largest inner product with the residual vector during an iteration, not only the index of that column but also the symmetrical index is added to the selected atom index matrix.

- Robustness

The correction method in Equation (5) is concerned with the amplitudes of the main peaks and lateral peaks. However, the OMP algorithm selects the atoms on which the residual vector achieves maximum projection. This strategy does not guarantee that the lateral peaks are selected. To address this issue, an additional iteration is applied in the OMP algorithm. This finds the index of the maximum peak and adds the atoms at the lateral peaks to the selected matrix if they are not selected.

The steps of the improved OMP for SMI signals are shown in Algorithm 1, and the differences from OMP are marked in red font.

Algorithm 1 The steps of improved OMP**Input:** Sensing matrix $\Theta \in \mathbb{R}^{M \times N}$; Sampling vector \mathbf{y} ; Maximum number of iterations m .**Initialization:** Number of iterations $t = 0$; Residual vector $\mathbf{r}_0 = \mathbf{y}$; Selected atom matrix $\Omega_0 = \emptyset$; Selected index matrix $\Lambda_0 = \emptyset$.**Iteration:**

```

1:   While  $t < m$ 
2:      $t = t + 1$ 
3:      $k_t = \arg \max_{n=1,2,\dots,N} \frac{|\langle \mathbf{r}_{t-1}, \Theta_n \rangle|}{\|\Theta_n\|_2}$ 
4:      $|\Lambda|_t = [\Lambda_{t-1} \ k_t \ k_{ts}]$ 
5:      $\Lambda_t = [\Omega_{t-1} \ \Theta_{k_t} \ \Theta_{k_{ts}}]$ 
6:      $\mathbf{S}_t = \arg \min_{\mathbf{S}} \|\Omega_t \mathbf{S} - \mathbf{Y}\|_2$ 
7:      $\mathbf{R}_t = \mathbf{Y} - \Omega_t \mathbf{S}_t$ 
8:   end while
9:    $\hat{\mathbf{S}}(\Lambda_t) = \mathbf{S}_t$ 
10:   $h = \arg \max_{n=1,2,\dots,N} \|\hat{\mathbf{S}}\|_2$ 
11:  if  $(h+1) \notin \Lambda_t$  or  $(h-1) \notin \Lambda_t$ 
12:     $\Lambda_{t+1} = [\Lambda_t \ h+1]$  or  $\Lambda_{t+1} = [\Lambda_t \ h-1]$ 
13:     $\Omega_{t+1} = [\Omega_t \ \Theta_{h+1}]$  or  $\Omega_{t+1} = [\Omega_t \ \Theta_{h-1}]$ 
14:     $\mathbf{S}_{t+1} = \arg \min_{\mathbf{S}} \|\Omega_{t+1} \mathbf{S} - \mathbf{Y}\|_2$ 
15:  end if

```

Output : $\hat{\mathbf{S}}(\Lambda_{t+1}) = \mathbf{S}_{t+1}$.

The improved OMP has the same input and initialization as the original OMP. The index k_t of a column called atom in the sensing matrix Θ that maximizes projections on the residual R is selected in Step 3. The index of the atom k_t and the atom itself Θ_{k_t} are added to the selected index matrix Ω and selected atom matrix Λ separately in Steps 4 and 5. In the improved algorithm, information concerning the symmetric atoms $\Theta_{k_{ts}}$ in the Fourier domain is also recorded. The recovered coefficient vector \mathbf{s} is calculated in Step 6 by solving a least-squares problem with the selected atoms, and the residual is calculated in Step 7. The operation from Step 2 to Step 7 repeats until the iteration index t reaches the maximum number of iterations m . To ensure that the atoms used for interpolated FFT in Equation (5) are all selected, the operations of Step 9 to Step 15 were added to the improved algorithm. The purpose is to judge whether the atom adjacent to the main peak has been selected; if not, it is added to the selected matrix, and the least-squares method is used to calculate the recovery coefficient again.

3. Experimental Results

To demonstrate the feasibility of using CS in SMI distance measurement, experiments to evaluate the difference between the traditional method and the CS method were implemented. The experimental setting used in this study was the same as the experimental equipment used in our previous study [10], which showed that when utilizing the conventional approach with interpolated FFT in the 3 to 20 cm range, a resolution of approximately 60 μm could be achieved at a signal-to-noise ratio of 30 dB. Figure 2 depicts the experimental setup.

A VCSEL HVS6003-001 laser diode with an integrated phototransistor was utilized in the experiment. It was modulated by a sawtooth current with amplitude of 2 mA and frequency of 50 Hz. The target was mounted on a translation stage, and the external distance between the target and the laser could be changed by adjusting the stage. The SMI signal was collected with the phototransistor and sampled using a data acquisition (DAQ) device after amplification and filtering. The sampling rate was set to 100 kHz. In this setting, 2000 data points could be extracted from each sawtooth period and 50 sets of data could be obtained in 1 s. Distance measurement was carried out at 10 different

positions in the range of 4 cm to 10 cm. The SMI signal of the laser modulated with the sawtooth wave is shown in Figure 3a, and the SMI signal extracted from the sawtooth edge is shown in Figure 3b.

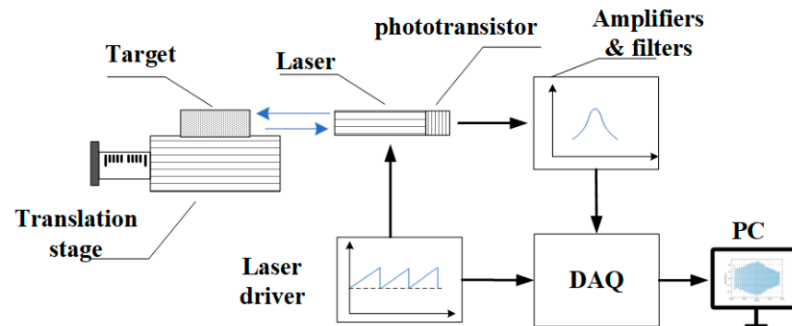


Figure 2. Schematic diagram of the experimental setup.

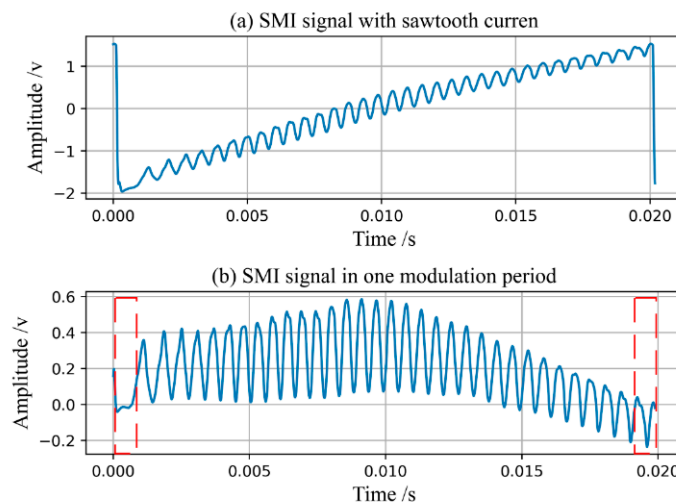


Figure 3. SMI signal: (a) Signal with sawtooth current; (b) Extracted SMI signals.

The cosine-like signal on the sawtooth wave in Figure 3a is the self-mixing signal, which could be extracted by subtracting the modulated sawtooth signal. The distance could be obtained via Equation (4) after calculating the frequency of the signal. In signal processing, 100 points in the dashed box at the beginning and end of each sawtooth period were removed to eliminate distortion in the SMI signal caused by the sudden change in the sawtooth signal.

In this experiment, a Gaussian random matrix was multiplied by the SMI signal to simulate the CS sampling process. For the CS method, the sampling size M was set to 300, and the maximum number of iterations m in the recovery algorithm was set to 50. The spectrum of the raw data s and the spectrum of the CS recovered data s' are shown in Figure 4a. The details of the non-zero values in the dashed box are shown in Figure 4b and the details of the zero values are shown in Figure 4c.

The results in Figure 4 show that most of the amplitudes of the SMI signal in the frequency domain were so small that they could be considered zero. In other words, the SMI signal could be regarded as sparse in the Fourier domain. Indexes with larger amplitudes were reconstructed and others were treated as zero in the recovery signal.

At each distance measurement, the data from 50 sawtooth cycles within one second was analyzed. The distance was calculated using both raw and recovered data. The difference between the calculated distances from two data sources was recorded. Figure 5 depicts the average difference and standard deviation of 50 measurements.

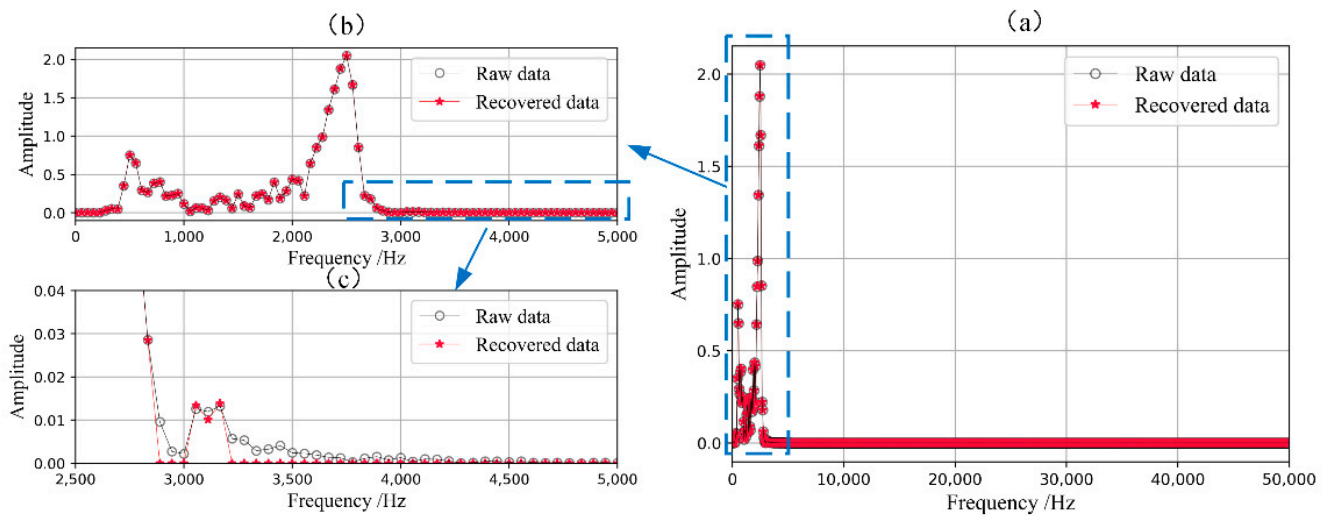


Figure 4. Spectra of raw and recovered data: (a) all spectrum data; (b) detail of non-zero values; (c) detail of zero values.

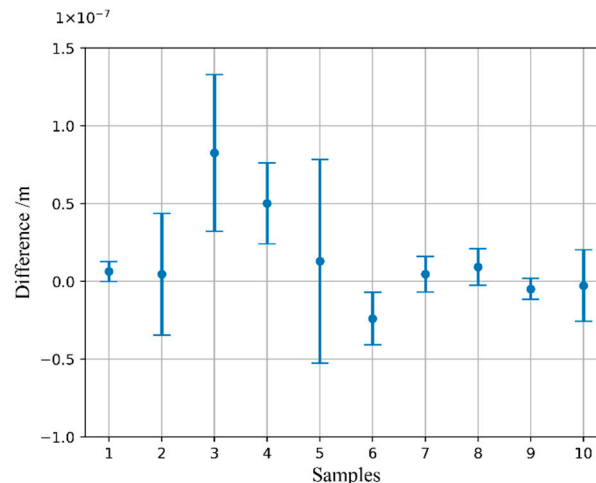


Figure 5. Differences in distance between raw data and CS recovery data.

The results in Figure 5 illustrate that the differences in distance between the CS method and the traditional method in the experiment were within $0.15 \mu\text{m}$. Compared with the measurement errors of approximately $60 \mu\text{m}$ in the distance measurement system using the traditional method, the differences caused by CS sampling were much smaller. Moreover, there were 300 points sampled to recover the SMI signal in the CS method, which was one-sixth of the original signal, with 1800 points. This means that the CS method is a promising technology in SMI distance measurement, achieving fewer samples at the expense of minor errors.

Some additional experiments were carried out to evaluate acceleration in the improved algorithm. The maximum number of iterations m was set to 100 and the residuals' norm $\|\mathbf{R}\|_2$ with and without acceleration were recorded. The change in residual is depicted in Figure 6.

Figure 6 shows that as the iteration index increased, the residual values became smaller. Residuals with acceleration dropped faster, indicating that the improved algorithm could recover the signal more quickly. The tendency of the residual values slowed down when the iteration index was greater than 50, so this value was used as the maximum number of iterations in our experiments.

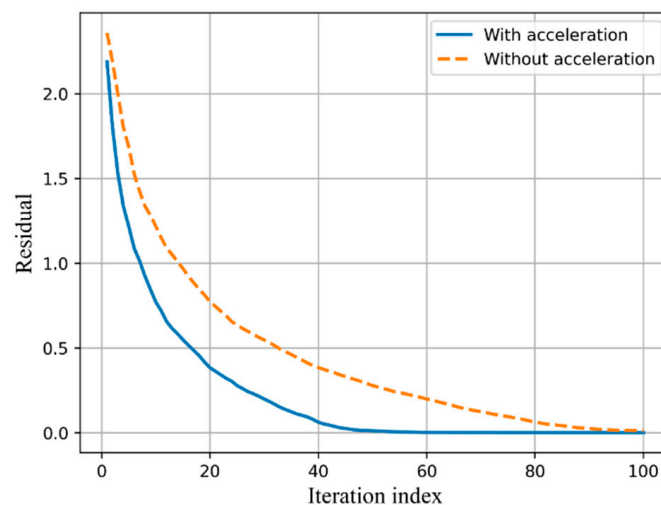


Figure 6. Change in residual versus iteration index.

4. Conclusions

An approach to distance measurement based on SMI using compressed sensing is proposed in this work. Compared with traditional methods, compressed sensing requires far fewer sampling points. Acceleration based on the symmetry of the Fourier spectrum was added to the recovery algorithm for faster convergence. In addition, considering the need for interpolated correction, atoms at specific positions were selected to guarantee the robustness of the algorithm. Distance measurements were carried out for assessing the feasibility of the proposed method. The results showed that the differences in distance between the traditional method with 1800 data points and the CS method with 300 data points were within 0.15 μm , which is minor when compared to the system measurement error of 60 μm . Further experiments will be carried out to verify the practical application of using the CS method on satellites. To sum up, the proposed approach provides a promising idea for SMI distance measurement using limited resources.

Author Contributions: Conceptualization, Y.D.; project administration, Y.Z. (Ye Zhu) and X.L.; writing—original draft preparation, L.L.; software and visualization, Y.Z. (Yue Zhang); writing—review and editing, X.Z. All authors have read and agreed to the published version of the manuscript.

Funding: This work was funded by the Strategic Priority Research Program of Chinese Academy of Sciences [grant number: XDA15020400], the Shanghai Municipal Science and Technology Major Project [grant number: 2019SHZDZX01], and the Science and Technology Innovation 2030—Quantum Communication and Quantum Computer [grant number: 2021ZD0300100].

Institutional Review Board Statement: Not applicable.

Informed Consent Statement: Not applicable.

Data Availability Statement: The data presented in this study are available upon request from the first author for noncommercial use.

Conflicts of Interest: The authors declare no conflict of interest.

References

1. Zhao, Y.; Fan, X.; Wang, C.; Lu, L. An Improved Intersection Feedback Micro-Radian Angle-Measurement System Based on the Laser Self-Mixing Interferometry. *Opt. Lasers Eng.* **2020**, *126*, 105866. [[CrossRef](#)]
2. Kou, K.; Wang, C.; Liu, Y. All-Phase FFT Based Distance Measurement in Laser Self-Mixing Interferometry. *Opt. Lasers Eng.* **2021**, *142*, 106611. [[CrossRef](#)]
3. Donati, S.; Norgia, M. Overview of Self-Mixing Interferometer Applications to Mechanical Engineering. *Opt. Eng.* **2018**, *57*, 051506. [[CrossRef](#)]
4. Barland, S.; Gustave, F. Convolutional Neural Network for Self-Mixing Interferometric Displacement Sensing. *Opt. Express* **2021**, *29*, 11433. [[CrossRef](#)] [[PubMed](#)]

5. Zhao, Y.; Xu, G.; Zhang, C.; Liu, K.; Lu, L. Vibration Displacement Immunization Model for Measuring the Free Spectral Range by Means of a Laser Self-Mixing Velocimeter. *Appl. Opt.* **2019**, *58*, 5540. [\[CrossRef\]](#)
6. Li, D.; Zhang, Z.; Huang, Z.; Wang, X.; Zhang, Z.; Huang, Z. Self-Mixing Interference Vibration Measurement Based on Even Equivalent Wavelength Fourier Transform Algorithm under Weak Feedback Regime. *Opt. Eng.* **2020**, *59*, 074101. [\[CrossRef\]](#)
7. Cui, X.; Li, C.; Geng, Y.; Ge, W.; Kan, L.; Zhang, Z. Secondary Envelope Extraction Based on Multiple Hilbert Transforms for Laser Self-Mixing Micro-Vibration Measurement. *Appl. Opt.* **2019**, *58*, 9392. [\[CrossRef\]](#)
8. Xiang, R.; Wang, C.; Lu, L. Laser Doppler Velocimeter Using the Self-Mixing Effect of a Fiber Ring Laser with Ultra-Narrow Linewidth. *J. Opt.* **2019**, *48*, 384–392. [\[CrossRef\]](#)
9. Lin, H.; Chen, J.; Xia, W.; Hao, H.; Guo, D.; Wang, M. Enhanced Self-Mixing Doppler Velocimetry by Fiber Bragg Grating. *Opt. Eng.* **2018**, *57*, 051504. [\[CrossRef\]](#)
10. Li, L.; Li, X.F.; Kou, K.; Wu, T.F. Approach of Self-Mixing Interferometry Based on Particle Swarm Optimization for Absolute Distance Estimation. *J. Opt. Soc. Korea* **2015**, *19*, 95–101. [\[CrossRef\]](#)
11. Donati, S.; Giuliani, G.; Merlo, S. Laser Diode Feedback Interferometer for Measurement of Displacements without Ambiguity. *IEEE J. Quantum Electron.* **1995**, *31*, 113–119. [\[CrossRef\]](#)
12. Sun, W.; Gui, H.; Zhang, P.; Wu, S.; Li, Z.; Zhang, K. Measuring Millimeter-Scale Distances in a Laser Self-Mixing Velocimeter with Low-Speed Wavelength Modulation. *Opt. Commun.* **2018**, *427*, 107–111. [\[CrossRef\]](#)
13. Norgia, M.; Magnani, A.; Pesatori, A. High Resolution Self-Mixing Laser Rangefinder. *Rev. Sci. Instrum.* **2012**, *83*, 045113. [\[CrossRef\]](#) [\[PubMed\]](#)
14. Zhao, Y.; Zhang, B.; Han, L. Laser Self-Mixing Interference Displacement Measurement Based on VMD and Phase Unwrapping. *Opt. Commun.* **2020**, *456*, 124588. [\[CrossRef\]](#)
15. Liu, J.; Huang, K.; Yao, X. Common-Innovation Subspace Pursuit for Distributed Compressed Sensing in Wireless Sensor Networks. *IEEE Sens. J.* **2019**, *19*, 1091–1103. [\[CrossRef\]](#)
16. Vinay, A.; Natarajan, S. Satellite Image Compression Using ROI Based EZW Algorithm. *Indones. J. Electr. Eng. Informatics* **2017**, *5*, 369–371. [\[CrossRef\]](#)
17. Zheng, T.; Dai, Y.; Xue, C.; Zhou, L. Recursive Least Squares for Near-Lossless Hyperspectral Data Compression. *Appl. Sci.* **2022**, *12*, 7172. [\[CrossRef\]](#)
18. Jiang, B.; Huang, G.; Li, F.; Zhang, S. Compressed Sensing with Dynamic Retransmission Algorithm in Lossy Wireless IoT. *IEEE Access* **2020**, *8*, 133827–133842. [\[CrossRef\]](#)
19. Zhou, F.; Zhao, L.; Li, L.; Hu, Y.; Jiang, X.; Yu, J.; Liang, G. GNSS Signal Acquisition Algorithm Based on Two-Stage Compression of Code-Frequency Domain. *Appl. Sci.* **2022**, *12*, 6255. [\[CrossRef\]](#)
20. Schoukens, J.; Pintelon, R.; Van Hamme, H. The Interpolated Fast Fourier Transform: A Comparative Study. *IEEE Trans. Instrum. Meas.* **1992**, *41*, 226–232. [\[CrossRef\]](#)
21. Kou, K.; Li, X.; Li, L.; Li, H.; Wu, T. Absolute Distance Estimation with Improved Genetic Algorithm in Laser Self-Mixing Scheme. *Opt. Laser Technol.* **2015**, *68*, 113–119. [\[CrossRef\]](#)
22. Zhang, C.; Zhang, R.; Zhu, Y.; Yang, H.; Shen, C.; Wei, S. Single-Shot Compressed Imaging via Random Phase Modulation. *Appl. Sci.* **2022**, *12*, 4536. [\[CrossRef\]](#)
23. Nouasria, H.; Et-tolba, M. A Fast Gradient-Based Sensing Matrix Optimization Approach for Compressive Sensing. *Signal Image Video Process.* **2022**. [\[CrossRef\]](#)
24. Candès, E.J.; Romberg, J.; Tao, T. Robust Uncertainty Principles: Exact Signal Reconstruction from Highly Incomplete Frequency Information. *IEEE Trans. Inf. Theory* **2006**, *52*, 489–509. [\[CrossRef\]](#)
25. Tropp, J.A.; Gilbert, A.C. Signal Recovery from Random Measurements via Orthogonal Matching Pursuit. *IEEE Trans. Inf. Theory* **2007**, *53*, 4655–4666. [\[CrossRef\]](#)
26. Tropp, J.A.; Laska, J.N.; Duarte, M.F.; Romberg, J.K.; Baraniuk, R.G. Beyond Nyquist: Efficient Sampling of Sparse Bandlimited Signals. *IEEE Trans. Inf. Theory* **2010**, *56*, 520–544. [\[CrossRef\]](#)